NANO LETTERS

LETTER

pubs.acs.org/NanoLett

Gradient Solvent Vapor Annealing of Block Copolymer Thin Films Using a Microfluidic Mixing Device

Julie N. L. Albert,[†] Timothy D. Bogart,[†] Ronald L. Lewis,[†] Kathryn L. Beers,[‡] Michael J. Fasolka,[‡] J. Brian Hutchison,[‡,§] Bryan D. Vogt,[‡,∥] and Thomas H. Epps, III[*,†]

[†]University of Delaware, Chemical Engineering Department, Newark, Delaware 19716, United States

[‡]Polymers Division, National Institute of Standards and Technology, Gaithersburg, Maryland 20899, United States

Supporting Information

ABSTRACT: Solvent vapor annealing (SVA) with solvent mixtures is a promising approach for controlling block copolymer thin film self-assembly. In this work, we present the design and fabrication of a solvent-resistant microfluidic mixing device to produce discrete SVA gradients in solvent composition and/or total solvent concentration. Using this device, we identified solvent composition dependent morphology transformations in poly(styrene-*b*-isoprene-*b*-styrene) films. This device enables faster and more robust exploration of SVA parameter space, providing insight into self-assembly phenomena.

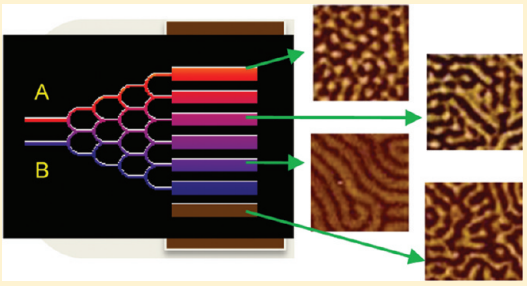

KEYWORDS: Gradients, solvent vapor annealing, block copolymer, thin film, self-assembly, microfluidic, mixing tree, nanostructure

The self-assembly of block copolymer thin films has garnered significant interest for emerging nanotechnologies,[1−5] including templating,[4−11] porous membranes,[12−15] organic optoelectronics,[16] and antireflection coatings.[17] In comparison to bulk systems, self-assembly in thin films (∼100 nm thickness) is strongly influenced by surface energetics and confinement effects.[1−4] Thus, many strategies for substrate surface modification[18−23] and controlled annealing conditions[24−28] have been utilized to manipulate block copolymer thin film morphology and nanostructure orientation.[1−4] In addition to understanding the thermodynamics of these self-assembling systems, identifying methods to kinetically trap desirable morphologies or nanostructure orientations is an attractive approach in some situations, such as obtaining perpendicularly orientated cylinders or lamellae for subsequent use as nanotemplates or nanoporous membranes.[9,29−31]

The characterization of bulk diblock copolymer morphologies has provided a foundation for understanding self-assembly according to the interactions between blocks, defined by the Flory−Huggins interaction parameter (χ), degree of polymerization (N), and block volume fractions (f).[32] More recent work has addressed the unique substrate and free surface effects present in thin film systems.[1,23,33−35] For example, surface energy, chemistry, and roughness have been shown to guide ordering from the substrate surface,[1,2,19,20,24,33,36−39] and thermal and solvent vapor annealing conditions have been employed to manipulate interactions at the free surface.[20,24,26,27,35,40,41]

Solvent vapor annealing (SVA) is a particularly attractive approach for controlling thin film self-assembly for several reasons. First, solvent vapor sorption into the film can mitigate substrate surface preferences thereby removing the need for substrate modifications (e.g., with a monolayer or brush layer) that could inhibit transport at the surface of conductive membranes or may be undesirable for templating applications.[9] Second, selective solvents can reduce preferential segregation of the lower surface tension block to the free surface and thereby create an effectively neutral surface[26,40] or even create a surface that preferentially attracts the higher surface tension block. This type of manipulation typically cannot be achieved with thermal annealing, unless the temperature dependence of the surface tensions enables a reversal of wetting preferences in an experimentally accessible range, such as for poly(styrene-*b*-methyl methacrylate) (PS-*b*-PMMA) thin films.[24,42] Third, SVA is typically conducted at room temperature, making it a valuable annealing technique for copolymers that are susceptible to thermal transitions or degradation.[43,44]

The use of solvent mixtures (versus a single solvent) offers an additional handle for tuning solvent selectivity and provides an avenue for achieving the desired block copolymer morphology. The solvent mixture approach has been successfully employed in systems such as poly(styrene-*b*-dimethylsiloxane) (PS-*b*-PDMS)/toluene/heptane[28] and poly(styrene-*b*-ethylene oxide) (PS-*b*-PEO)/benzene/water (controlled humidity);[27,35] however, the SVA parameter space, consisting of solvent choice, total solvent concentration/swollen film thickness, and solvent removal rate, remains largely unexplored.

Received: December 23, 2010
Revised: January 23, 2011
Published: February 09, 2011

In this work, we present the design, fabrication, and use of a solvent resistant microfluidic mixing device that produces discrete gradients in solvent vapor composition and/or concentration. This device also enables real-time monitoring of film thickness to quickly explore the SVA parameter space and the accompanying self-assembly phenomena.

Self-assembly during SVA is the result of several complex phenomena.[3] First, the selectivity of the solvent vapor(s) will establish surface preference at the free surface; for example, if the solvent prefers one of the blocks, the free surface becomes preferential for that block.[26,40,45−47] Second, vapor sorption into the film effectively lowers the glass transition temperature of each block and increases chain mobility;[27,40,44,47,48] this effect is especially important when annealing copolymers containing blocks that are glassy at room temperature, such as poly(styrene) and poly(methyl methacrylate). Third, interactions between blocks and the relative block volume fractions are affected by the solvent within the film, which can lead to morphology transformations.[26,28,35,40,44,46−50] Fourth, solvent−substrate interactions can screen undesirable polymer−substrate interactions[27,40,51,52] or cause film dewetting.[33] Finally, film swelling can impact domain spacing (L_0) and film thickness commensurability considerations.[3,48,52]

Table 1. Solubility Parameters of Materials and Solvents Examined[56]

material	solubility parameter ($MPa^{1/2}$)
n-hexane	14.9
THF	19.4
PI	16.6[a]
PS	18.4[b]

[a] Average value; data range: 16.2 to 17.1 $MPa^{1/2}$. [b] Average value; data range: 17.5 to 19.3 $MPa^{1/2}$.

For our studies, a poly(styrene-*b*-isoprene-*b*-styrene) (SIS) (DEXCO SIS v4211)[53] copolymer was selected as a model system for examining self-assembly due to its well-defined bulk morphology (hexagonally packed cylinders) and its applicability to nanotemplating due to facile removal of the poly(isoprene) block.[54] The SIS polymer had an overall molecular mass of 118 kg/mol, block volume fractions of $f_S = 0.134$, $f_I = 0.732$, $f_S = 0.134$, a polydispersity index of 1.09, and a bulk domain spacing of 29 nm. SIS thin films were flow coated[55] from tetrahydrofuran (THF) on toluene-rinsed, ultraviolet-ozone (UVO)-treated silicon wafers. Two solvents were chosen for gradient annealing: *n*-hexane, which is preferential for the poly(isoprene) (PI) block and a poor solvent for the poly(styrene) (PS) block, and THF, which is slightly preferential for the PS block but a good solvent for both blocks.[56] The solubility parameters of these materials are listed in Table 1.

Solvent-resistant mixing devices were fabricated using photopolymerizable materials as outlined in Figure 1. First, poly(dimethylsiloxane) (PDMS) spacers were made from an elastomer base and curing agent (Sylgard 184 Silicone Elastomer) mixed in a 10:1 ratio by mass, degassed under vacuum for 1 h, poured into a mold, and cured overnight at 80 °C under atmospheric conditions. Rectangular spacers 6.35 mm (1/4 in.) thick were cut from the cured elastomer. Next, the design masks for solvent annealing and solvent collection (see Figure 2) were printed on transparencies and affixed to a microscope slide for support. The design masks incorporated two "injection ports" for solvent entry into the device, a "mixing tree" to facilitate mixing of the solvent vapors and produce a gradient in composition, and "annealing chambers" where the polymer film was exposed to the solvent vapor for annealing. Additionally, a control chamber, which was not connected to the mixing tree, was used to show that lateral diffusion of solvent vapors through the device walls was negligible (see Figure 2a). Finally, "outlet ports" on the solvent collection device (see Figure 2b) were used to connect the

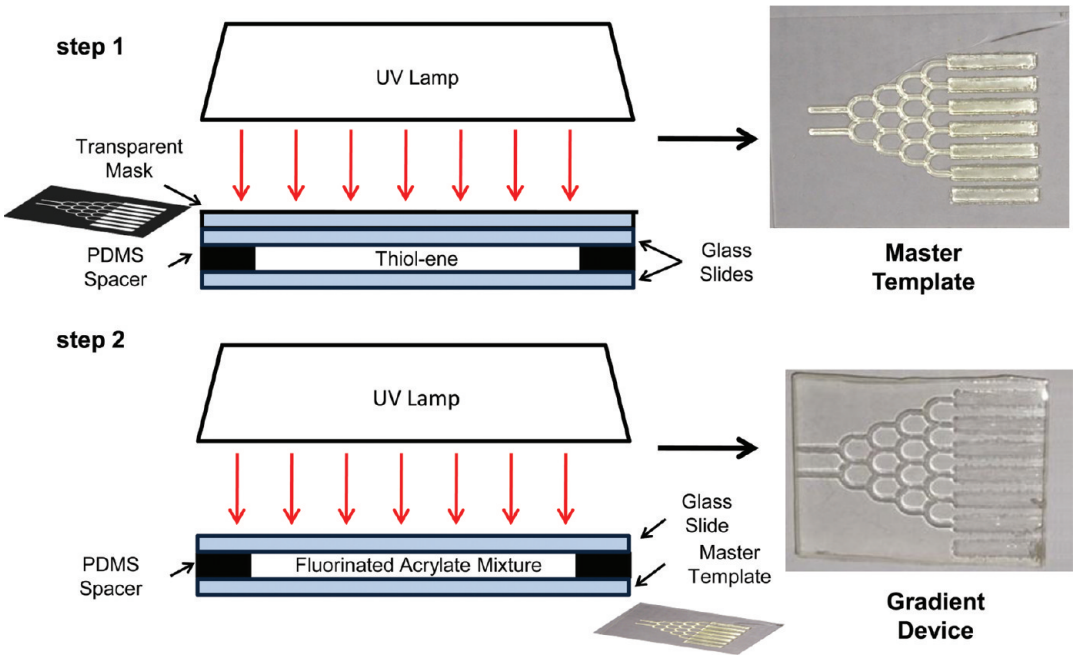

Figure 1. Microfluidic device fabrication steps. (Step 1) Frontal photopolymerization of thiol−ene yields a master template (with features ≈750 μm in height) of the device design. (Step 2) The master template is used to pattern channels in the device during photopolymerization of a fluorinated acrylate mixture.

dx.doi.org/10.1021/nl104496r |*Nano Lett.* 2011, 11, 1351–1357

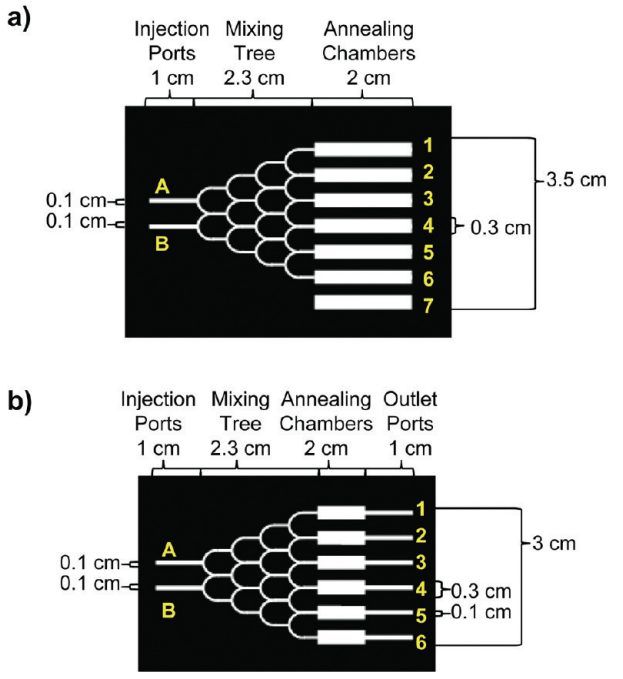

Figure 2. Design masks for (a) the solvent annealing device and (b) the solvent collection device. In the final devices, solvent vapors enter through injection ports A and B, mix in the mixing tree, and pass through annealing chambers 1−6. In the solvent annealing device, chamber 7 is detached from the mixing tree and serves as a control chamber. In the solvent collection device, the outlet ports are connected to chilled collection vials.

annealing chambers to chilled collection vials for subsequent analysis of the vapor composition in the annealing chambers.

Master templates were created by frontal photopolymerization of thiol−ene resin (Norland Optical Adhesive 81).[57,58] Thiol-ene resin was sandwiched between two clean glass slides (rinsed with ethanol, UVO-treated), the design mask was placed on top of the sandwich, and the system was exposed to UV irradiation (Spectroline Model SB-100PD, 365 nm, 0.75 mW/cm^2) for 45 s (see Figure 1). The resulting master template (with features ≈750 μm in height) was cleaned with ethanol and a 2:1 by volume ethanol:acetone mixture and irradiated for an additional 5 min postcure.

Microfluidic devices were fabricated from the master templates using a mixture of fluorinated oligomer (CN4000) (Sartomer Company, CN4000),[59] 1H,1H-perfluoro-*n*-decyl acrylate (PFDA) (ExFluor Research Corp.), and 2,2-dimethoxy-2-phenylacetophenone (photoinitiator) (Acros Organics) mixed in a 2:1 ratio by mass of PFDA:CN4000 with 0.15 mass % photoinitiator. The fluorinated acrylate mixture was sandwiched between the master template and a clean glass slide. UV irradiation for 16 min (365 nm, 0.75 mW/cm^2) cured the mixture, resulting in a stiff yet rubbery, solvent-resistant device with the imprinted channels.

The solvent annealing device was used to anneal substrate-supported SIS films, and the composition of the mixed solvent vapor flowing through each annealing chamber was assessed from multiple solvent collection runs. For both solvent annealing and solvent collection, the device and substrate were clamped between two glass slides to provide a seal between the imprinted side of the device and the silicon substrate. Only the "annealing chamber" region of the device covered the

Table 2. Fraction of *n*-Hexane Vapor Normalized by the Total Solvent Vapor that Passed through Each Annealing Chamber, the Remainder being THF[a]

chamber	*n*-hexane fraction
1	>0.99
2	>0.99
3	0.99 ± 0.01
4	0.98 ± 0.01
5	0.93 ± 0.04
6	0.69 ± 0.08

[a] The error reported represents one standard deviation of the data from nine repeated solvent collection runs and is taken as the experimental uncertainty of the measurement.

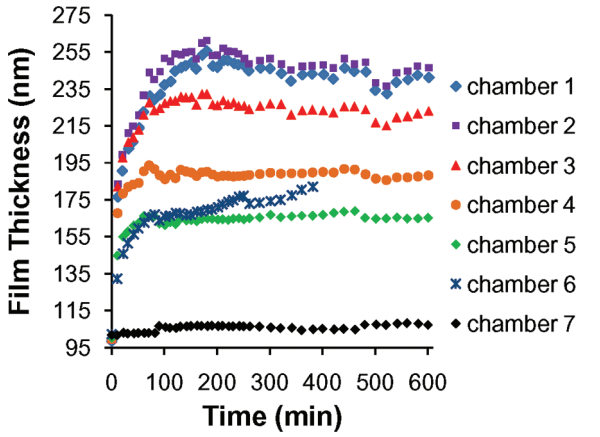

Figure 3. Thickness of the polymer film within each chamber as a function of annealing time. Lower chamber numbers contained higher fractions of *n*-hexane (Table 2). Measurements were taken at the "beginning" of each chamber (∼4−6 mm from the point of solvent entry). The experimental uncertainty of each measurement is ±1 nm as estimated from repeated measurements on an unswollen film of constant thickness; error bars (not shown) are the same size as the data markers. Chamber 6 data ends at ∼390 min because the film dewet. Chamber 7 was detached from the mixing tree and served as a control chamber.

polymer film. A nitrogen carrier gas was bubbled through each of the selected solvents at rates of 10.6 ± 0.2 mL/min (*n*-hexane, vapor pressure ≈150 mm Hg at 25 °C)[60] and 1.9 ± 0.1 mL/min (THF, vapor pressure ≈161 mm Hg at 25 °C)[60] providing solvent-enriched streams to the inlet ports of the device. Flow rates were chosen based on preliminary work, which showed that interesting morphological transformations occur in our SIS system at high *n*-hexane concentrations.

For solvent collection, the ends of the chambers were connected to individual chilled collection vials (−40 to −60 °C) into which solvent vapor was condensed and collected for 24 h. The nitrogen carrier gas was vented from the vials during the collection. The composition of solvent collected from each chamber was analyzed by proton nuclear magnetic resonance (^{1}H NMR) using deuterated chloroform as the solvent (Table 2). Representative ^{1}H NMR spectra from one solvent collection run are provided in the Supporting Information (Figure S1). Solvent collection was performed on substrates with and without the polymer film, and no significant difference

dx.doi.org/10.1021/nl104496r |*Nano Lett.* 2011, 11, 1351–1357

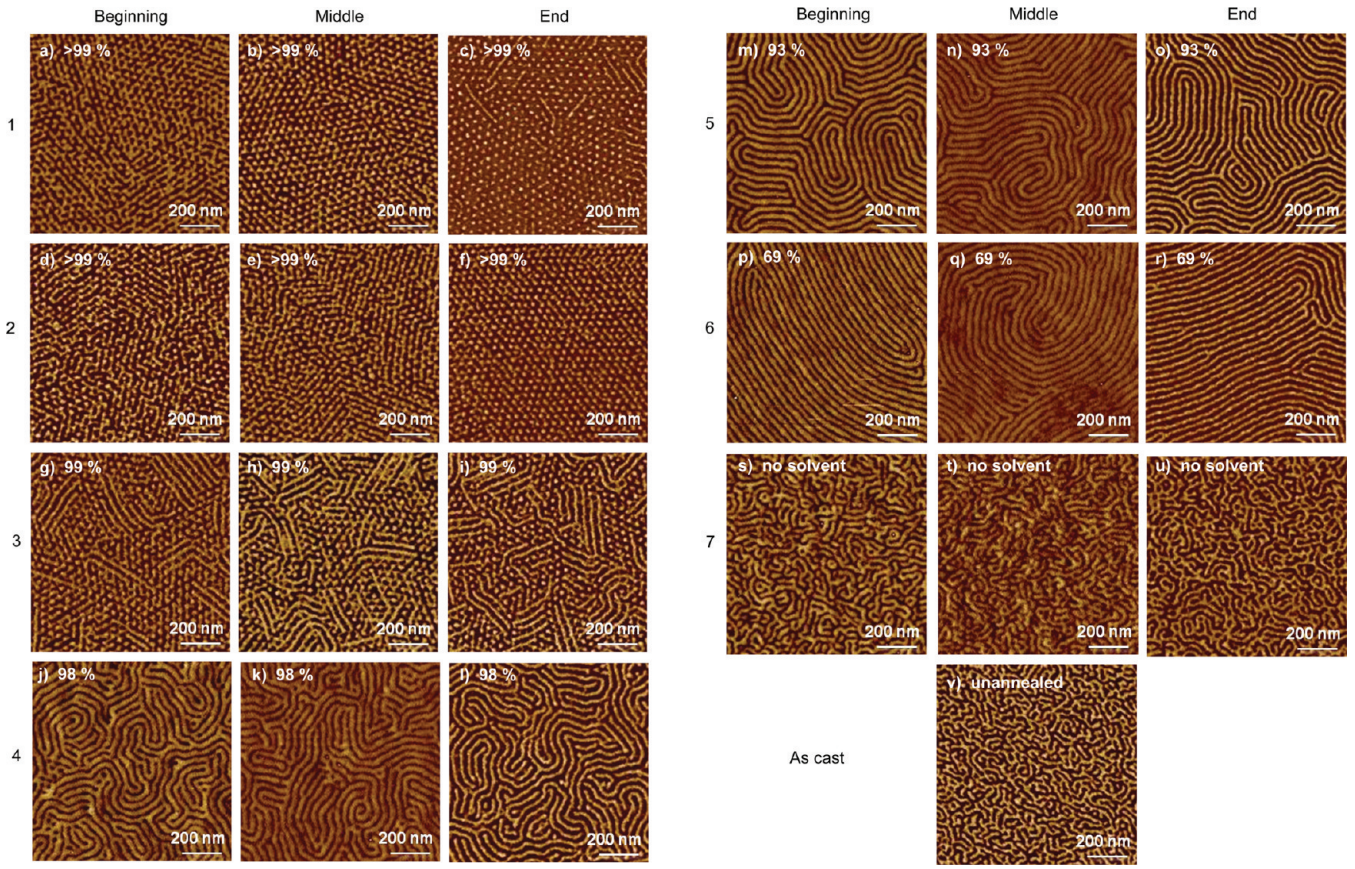

Figure 4. AFM phase images of a polymer film after device annealing. Chamber number is indicated on the left, position within the chamber is indicated at the top, and solvent vapor composition (% *n*-hexane) is listed with each image.

in the composition of solvent collected was found between the two cases.

For solvent annealing, holes were cut in the top of each chamber, and the upper glass slide was replaced with a quartz slide to enable in situ film thickness measurements using spectral reflectance (Filmetrics, Inc. F20−UV) during the anneal (see Figure 3). The ends of the chambers were left open to the atmosphere. The initial thickness of the SIS thin film was 100 ± 2 nm, and the film formed a mixed morphology of perpendicular and parallel PS cylinders in a PI matrix prior to SVA (see Figure 4v).

Figure 3 shows how the film thickness evolved during a 10 h anneal. During solvent annealing, the refractive index of the film was lowered due to solvent sorption into the polymer.[48] To interpret reflectance spectra, linear combinations of previously determined refractive index profiles for SIS films swollen with pure *n*-hexane or pure THF were used to fit the film thickness (see Supporting Information for additional detail).

Chambers 1 through 5 appeared to reach a steady-state condition after approximately 100 min as the film thicknesses fluctuated around average values throughout the remainder of the anneal. Chambers 1 and 2 were effectively swollen with the same amount of solvent (∼60 vol % of the ≈245 nm total film thickness is attributable to the solvent), and the level of swelling decreased down to ∼40 vol % solvent (≈165 nm total film thickness) in chamber 5. This trend was expected because the total flow from the *n*-hexane bubbler entering the device was approximately five times the flow entering from the THF bubbler. Unlike chambers 1 through 5, the film thickness in chamber 6 increased continuously until the film dewet when swollen with ≈45 vol % solvent (≈180 nm total film thickness) after 390 min. In contrast, the control chamber (chamber 7) showed effectively no change in thickness, which indicated that minimal solvent diffusion occurred through the device walls.

At the end of the SVA, the device was quickly removed from the polymer film so that fast evaporation of solvent (<10 s) would trap the annealed morphologies.[11,27,30,35,47,49] Atomic force microscopy (AFM) phase images (see Figure 4) were obtained from three positions on the film within each chamber. Hereafter, "beginning", "middle", and "end" refer to locations ≈4−6 mm into the chamber from the point of solvent entry, ≈10−12 mm into the chamber, and ≈16−18 mm into the chamber, respectively. From these AFM micrographs of the polymer top surface, the morphology of the film under these SVA conditions could not be determined unequivocally. However, the high throughput mixing tree approach allowed us to identify the compositions of interest where phase transformations occurred. In the following paragraphs, we discuss these results based on free energy, effective volume fraction, and chain mobility arguments.

First, comparison of the images from different positions within a chamber indicated that the chamber opening subtly affected the morphology. In chambers 1 and 2, hexagonal order improved from the beginning to the end of each chamber (see Figure 4a−c, d−f). In chambers 3−6, the number of defects increased slightly from the beginning to the end of the chamber (see Figure 4g−i, j−l,m−o,p−r). (Note: the phase inversions in the AFM images of Figure 4l,o,r are due to imaging artifacts, not an inversion of

dx.doi.org/10.1021/nl104496r |*Nano Lett.* 2011, 11, 1351–1357

the block phases.[61]) This occurrence could be explained by differences in chain mobility, which suggested that the solvent concentration in the film may have been lower near the end of the chamber compared to the beginning.

Second, as the ratio of *n*-hexane to THF decreased and swollen film thickness decreased, AFM results were consistent with a morphology transformation from structures containing mostly perpendicular cylinders or spheres at the surface (chambers 1, 2, and 3; see Figure 4a−i) to parallel cylinder structures with increasing long-range order (chambers 4, 5, and 6; see Figure 4j−r). The morphology in chamber 7 was similar to the as-cast morphology (see Figure 4s−u,v), confirming that minimal solvent diffusion occurred through the device walls.

The high concentration of PI-selective *n*-hexane vapor could promote either spherical or perpendicular cylinder morphologies in the first few chambers based on effective volume fraction and free energy arguments, respectively. These driving forces could also support hybrid morphologies, such as a perpendicular-on-parallel cylinder morphology.[62] The AFM micrographs taken from the beginning of chambers 1 and 2 (see Figure 4a,d) were consistent with such a hybrid morphology.

To examine the effective volume fraction argument in more detail, a simplified mass conservation calculation (neglecting differences in solvent and polymer densities) was employed. If for example ≈85−90% of the solvent in the film partitioned to the PI domain (≈10−15% higher than the initial copolymer f_I), then the new volume fraction of the PI domain would be ≈0.78−0.80. In bulk AB diblock theoretical phase diagrams, this composition corresponds to a spherical morphology;[63,64] the similarities between ABA triblock and AB diblock copolymer phase behavior are well-established.[65] Additionally, this level of partitioning would still allow sufficient swelling of the PS domain (≈18−25% solvent in the domain) to provide PS chain mobility for reorganization.[66] Thus, a phase transformation from cylinders to spheres in this SIS system could be thermodynamically favored.

The rationale for perpendicular cylinders is more complex. Surface energy arguments favor segregation of the PI block to the free surface, both due to its lower surface tension relative to PS and due to the preference of *n*-hexane for the PI block. However because PI is the middle block in the ABA architecture, formation of a PI wetting layer at the free surface would require entropically unfavorable looping of chains at this interface. We hypothesize that avoidance of this entropic penalty by expression of both blocks at the free surface may be more energetically favorable than wetting layer formation. On the basis of geometrical arguments, more of the PI block (less of the PS block) would be expressed at the free surface for a perpendicular cylinder morphology compared to a parallel morphology with half-cylinders of PS at the surface (see Supporting Information, Figure S2).

As the *n*-hexane content of the vapor decreased, both the driving forces for spherical or perpendicular cylinder containing morphologies would be reduced. Consistent with this proposition, parallel cylinders began to appear at the surface of the film in chamber 3, producing a mixed morphology. Reduced chain mobility due to lower film swelling in chamber 3 compared with chambers 1 and 2 may also have contributed to the mixed structure. With these data, we cannot determine whether the system energetics favor both morphologies equally such that fluctuations lead to coexistence, or whether a pure perpendicular cylinder/sphere or parallel cylinder morphology would emerge if the film was annealed longer.

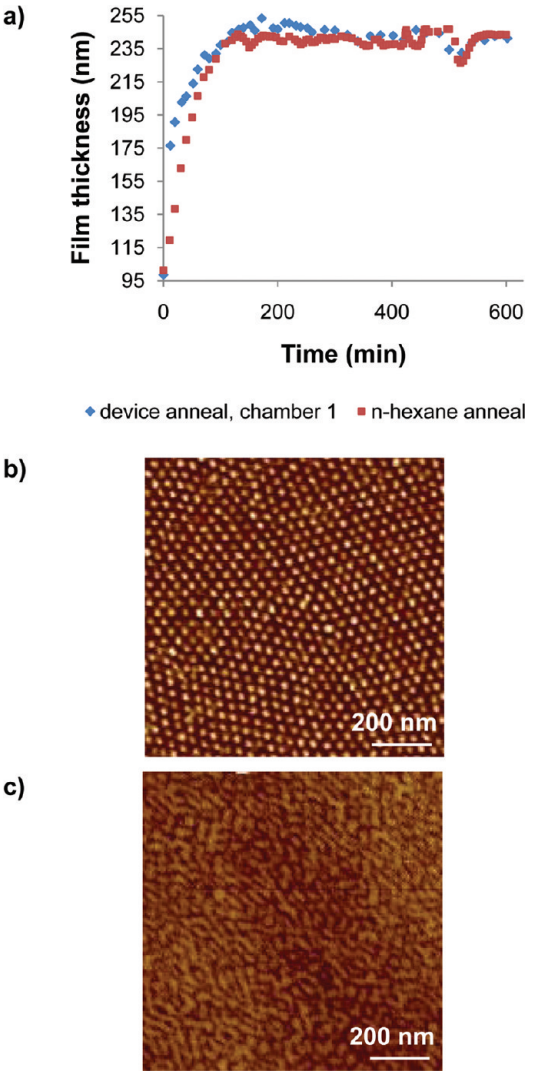

Figure 5. (a) Comparison of film thickness profiles for the SIS film in chamber 1 of the device anneal and the scaled-up *n*-hexane annealed film. The experimental uncertainty of each measurement is ±1 nm as estimated from repeated measurements on an unswollen film of constant thickness; error bars (not shown) are the same size as the data markers. (b) AFM phase image of the top of the *n*-hexane annealed film. Like the film in chamber 1 of the device anneal, the morphology was consistent with spheres, perpendicular cylinders, or a hybrid morphology. (c) AFM phase image of the underside of the *n*-hexane annealed film, suggesting that a hybrid morphology is likely.

With a small decrease in the *n*-hexane vapor composition to 98% (increase in THF vapor to 2%), parallel cylinders were promoted in chamber 4. Despite a much lower solvent concentration in the film compared to chamber 3 (47 vol% solvent in film versus 56 vol% solvent in film), the parallel cylinders found in chamber 4 were well-ordered; this order illustrates the ability of THF, a good solvent for both the PS and PI blocks, to impart chain mobility. With further decreasing *n*-hexane (increasing THF) concentration, the parallel cylinders in chambers 5 and 6 achieved better long-range order compared with chamber 4, again despite a lower overall solvent concentration in the film.

Finally, chamber 6 had the lowest *n*-hexane (highest THF) concentration, and the polymer film partially dewet during the experiment. Dewetting of the film from the substrate surface was

dx.doi.org/10.1021/nl104496r |*Nano Lett.* 2011, 11, 1351–1357

likely due to the affinity of the polar THF molecules for the native oxide of the silicon substrate.

For a more thorough assessment of the morphology of the SVA films, the annealing conditions created by the gradient device were readily reproduced on a larger scale with an annealing setup described by Cavicchi et al.[52] to produce film sample sizes appropriate for more intensive study and morphology characterization. We demonstrated this scale-up by mimicking the annealing conditions in chamber 1, which showed the most interesting phase behavior. The solvent vapor consisted of only *n*-hexane (chamber 1 composition was >99% *n*-hexane), and the total solvent concentration was controlled by the relative flow rates of a solvent-enriched stream and a pure nitrogen stream. Figure 5a shows that the film thickness profile for the scaled-up *n*-hexane annealed film was nearly identical to the film thickness evolution in chamber 1 of the device anneal. AFM phase images of the scaled-up *n*-hexane annealed film were also consistent with the morphology in chamber 1 of the device anneal (see Figures 5b and 4a−c). Additionally, a section of the film was peeled off of the substrate for imaging using a technique described by Fasolka et al.[39] and Epps et al.[33] AFM phase images of the underside of the film supported identification of a possible hybrid morphology, such as perpendicular-on-parallel cylinders (see Figure 5c).

In summary, we have presented the design, fabrication, and use of a solvent resistant microfluidic mixing device that produces discrete gradients in solvent vapor composition and/or solvent vapor concentration to efficiently explore SVA parameter space and the resulting block copolymer self-assembly. The device also enables real-time monitoring of film thickness for measuring solvent uptake by the film. Because of the facile fabrication and implementation of this device, the gradient SVA approach is now readily accessible for traditional systems, such as the SIS thermoplastic elastomer examined here, as well as novel multiblock, branched, and conductive copolymer systems. The device can be used to identify microstructures and morphology transformations of interest for more intensive study and characterization with techniques such as grazing incidence small-angle X-ray scattering, cross-sectional imaging, or combinatorial thin film removal methods.[67] Furthermore, critical analysis of morphological transformations and dewetting phenomena as a function of solvent selectivity and concentration in all polymer systems will improve understanding of the interplay between confinement effects and surface and interfacial interactions that guide block copolymer thin film self-assembly.

■ ASSOCIATED CONTENT

Supporting Information. ^{1}H NMR spectra from a representative solvent collection run. Fitting reflectance spectra for film thickness determination. Geometrical argument for perpendicular cylinder morphology. This material is available free of charge via the Internet at http://pubs.acs.org.

■ AUTHOR INFORMATION

Corresponding Author

*E-mail: thepps@udel.edu.

Present Addresses

[§]RainDance Technologies, Inc., Lexington, MA 02421.

[∥]Chemical Engineering Program, Arizona State University, Tempe, AZ 85284.

■ ACKNOWLEDGMENT

This work was supported by the National Science Foundation (NSF) through DMR-0645586 and an NSF Graduate Research Fellowship to J.N.L.A. ^{1}H NMR spectra were obtained with instrumentation supported by NSF CRIF: MU, CHE 0840401. We acknowledge the W. M. Keck Electron Microscopy Facility for use of their atomic force microscopes. We also thank Dr. B. M. Vogel (Bucknell University) and J. F. Elman (Filmetrics, Inc.) for insightful discussions.

■ REFERENCES

(1) Fasolka, M. J.; Mayes, A. M. *Annu. Rev. Mater. Res.* **2001**, *31*, 323–355.

(2) Segalman, R. A. *Mater. Sci. Eng., R* **2005**, *48* (6), 191–226.

(3) Albert, J. N. L.; Epps, T. H., III *Mater. Today* **2010**, *13* (6), 24–33.

(4) Bang, J.; Jeong, U.; Ryu, D. Y.; Russell, T. P.; Hawker, C. J. *Adv. Mater.* **2009**, *21*, 4769–4792.

(5) Marencic, A. P.; Register, R. A. *Annu. Rev. Chem. Biomol. Eng.* **2010**, *1* (1), 277–297.

(6) Urade, V. N.; Wei, T. C.; Tate, M. P.; Kowalski, J. D.; Hillhouse, H. W. *Chem. Mater.* **2007**, *19* (4), 768–777.

(7) Crossland, E. J. W.; Kamperman, M.; Nedelcu, M.; Ducati, C.; Wiesner, U.; Smilgies, D. M.; Toombes, G. E. S.; Hillmyer, M. A.; Ludwigs, S.; Steiner, U.; Snaith, H. J. *Nano Lett.* **2008**, *9* (8), 2807–2812.

(8) Ruiz, R.; Kang, H.; Detcheverry, F. A.; Dobisz, E.; Kercher, D. S.; Albrecht, T. R.; De Pablo, J. J.; Nealey, P. F. *Science* **2008**, *321*, 936–939.

(9) Park, S.; Wang, J.-Y.; Kim, B.; Xu, J.; Russell, T. P. *ACS Nano* **2008**, *2* (4), 766–772.

(10) Park, M.; Harrison, C.; Chaikin, P. M.; Register, R. A.; Adamson, D. H. *Science* **1997**, *276* (5317), 1401–1404.

(11) Rodwogin, M. D.; Spanjers, C. S.; Leighton, C.; Hillmyer, M. A. *ACS Nano* **2010**, *4* (2), 725–732.

(12) Thurn-Albrecht, T.; Steiner, R.; DeRouchey, J.; Stafford, C. M.; Huang, E.; Bal, M.; Tuominen, M.; Hawker, C. J.; Russell, T. P. *Adv. Mater.* **2000**, *12* (11), 787–791.

(13) Olson, D. A.; Chen, L.; Hillmyer, M. A. *Chem. Mater.* **2007**, *20* (3), 869–890.

(14) Yang, S. Y.; Ryu, I.; Kim, H. Y.; Kim, J. K.; Jang, S. K.; Russell, T. P. *Adv. Mater.* **2006**, *18* (6), 709–712.

(15) Phillip, W. A.; O'Neill, B.; Rodwogin, M.; Hillmyer, M. A.; Cussler, E. L. *Appl. Mater. Interfaces* **2010**, *2* (3), 847–853.

(16) Segalman, R. A.; McCulloch, B.; Kirmayer, S.; Urban, J. J. *Macromolecules* **2009**, *42* (23), 9205–9216.

(17) Joo, W.; Park, M. S.; Kim, J. K. *Langmuir* **2006**, *22* (19), 7960–7963.

(18) Genzer, J.; Bhat, R. R. *Langmuir* **2008**, *24* (6), 2294–2317.

(19) Albert, J. N. L.; Baney, M. J.; Stafford, C. M.; Kelly, J. Y.; Epps, T. H., III *ACS Nano* **2009**, *3* (12), 3977–3986.

(20) Mansky, P.; Liu, Y.; Huang, E.; Russell, T. P.; Hawker, C. *Science* **1997**, *275* (5305), 1458–1460.

(21) In, I.; La, Y.-H.; Park, S.-M.; Nealey, P. F.; Gopalan, P. *Langmuir* **2006**, *22* (18), 7855–7860.

(22) Peters, R. D.; Yang, X. M.; Kim, T. K.; Nealey, P. F. *Langmuir* **2000**, *16*, 9620–9626.

(23) Smith, A. P.; Sehgal, A.; Douglas, J. F.; Karim, A.; Amis, E. J. *Macromol. Rapid Commun.* **2003**, *24* (1), 131–135.

(24) Han, E.; Stuen, K. O.; Leolukman, M.; Liu, C.-C.; Nealey, P. F.; Gopalan, P. *Macromolecules* **2009**, *42* (13), 4896–4901.

(25) Mansky, P.; Russell, T. P.; Hawker, C. J.; Mays, J.; Cook, D. C.; Satija, S. K. *Phys. Rev. Lett.* **1997**, *79* (2), 237–240.

(26) Xuan, Y.; Peng, J.; Cui, L.; Wang, H.; Li, B.; Han, Y. *Macromolecules* **2004**, *37* (19), 7301–7307.

(27) Kim, S. H.; Misner, M. J.; Xu, T.; Kimura, M.; Russell, T. P. *Adv. Mater.* **2004**, *16* (3), 226–231.
(28) Jung, Y. S.; Ross, C. A. *Adv. Mater.* **2009**, *21* (24), 2540–2545.
(29) Kim, G.; Libera, M. *Macromolecules* **1998**, *31* (8), 2670–2672.
(30) Phillip, W. A.; Hillmyer, M. A.; Cussler, E. L. *Macromolecules* **2010**, *43* (18), 7763–7770.
(31) Peng, J.; Kim, D. H.; Knoll, W.; Xuan, Y.; Li, B.; Han, Y. *J. Chem. Phys.* **2006**, *125*, No. 064702.
(32) Bates, F. S. *Science* **1991**, *251* (4996), 898–905.
(33) Epps, T. H., III; DeLongchamp, D. M.; Fasolka, M. J.; Fischer, D. A.; Jablonski, E. L. *Langmuir* **2007**, *23* (6), 3355–3362.
(34) Han, E.; Stuen, K. O.; La, Y.-H.; Nealey, P. F.; Gopalan, P. *Macromolecules* **2008**, *41* (23), 9090–9097.
(35) Bang, J.; Kim, B. J.; Stein, G. E.; Russell, T. P.; Li, X.; Wang, J.; Kramer, E. J.; Hawker, C. J. *Macromolecules* **2007**, *40* (19), 7019–7025.
(36) Segalman, R. A.; Yokoyama, H.; Kramer, E. J. *Adv. Mater.* **2001**, *13* (15), 1152–1155.
(37) Sivaniah, E.; Hayashi, Y.; Matsubara, S.; Kiyono, S.; Hashimoto, T.; Fukunaga, K.; Kramer, E. J.; Mates, T. *Macromolecules* **2005**, *38* (5), 1837–1849.
(38) Rockford, L.; Liu, Y.; Mansky, P.; Russell, T. P.; Yoon, M.; Mochrie, S. G. J. *Phys. Rev. Lett.* **1999**, *82* (12), 2602–2605.
(39) Fasolka, M. J.; Harris, D. J.; Mayes, A. M.; Yoon, M.; Mochrie, S. G. J. *Phys. Rev. Lett.* **1997**, *79* (16), 3018–3021.
(40) Cavicchi, K. A.; Berthiaume, K. J.; Russell, T. P. *Polymer* **2005**, *46* (25), 11635–11639.
(41) Huang, E.; Russell, T. P.; Harrison, C.; Chaikin, P. M.; Register, R. A.; Hawker, C. J.; Mays, J. *Macromolecules* **1998**, *31* (22), 7641–7650.
(42) Mansky, P.; Russell, T. P.; Hawker, C. J.; Pitsikalis, M.; Mays, J. *Macromolecules* **1997**, *30* (22), 6810–6813.
(43) Kelly, J. Y.; Albert, J. N. L.; Howarter, J. A.; Kang, S.; Stafford, C. M.; Epps, T. H., III; Fasolka, M. J. *ACS Appl. Mater. Interfaces* **2010**, *2* (11), 3241–3248.
(44) Di, Z.; Posselt, D.; Smilgies, D.-M.; Papadakis, C. M. *Macromolecules* **2009**, *43* (1), 418–427.
(45) Lin, Z. Q.; Kim, D. H.; Wu, X. D.; Boosahda, L.; Stone, D.; LaRose, L.; Russell, T. P. *Adv. Mater.* **2002**, *14* (19), 1373–1376.
(46) Knoll, A.; Horvat, A.; Lyakhova, K. S.; Krausch, G.; Sevink, G. J. A.; Zvelindovsky, A. V.; Magerle, R. *Phys. Rev. Lett.* **2002**, *89* (3), No. 035501.
(47) Knoll, A.; Magerle, R.; Krausch, G. *J. Chem. Phys.* **2004**, *120* (2), 1105–1116.
(48) Zettl, U.; Knoll, A.; Tsarkova, L. *Langmuir* **2010**, *26* (9), 6610–6617.
(49) Chen, Y.; Huang, H.; Hu, Z.; He, T. *Langmuir* **2004**, *20* (9), 3805–3808.
(50) Li, Y.; Huang, H.; He, T.; Gong, Y. *J. Phys. Chem. B* **2010**, *114* (3), 1264–1270.
(51) Kim, S.; Briber, R. M.; Karim, A.; Jones, R. L.; Kim, H. C. *Macromolecules* **2007**, *40* (12), 4102–4105.
(52) Cavicchi, K. A.; Russell, T. P. *Macromolecules* **2007**, *40* (4), 1181–1186.
(53) Certain commercial materials and equipment are identified in this paper in order to specify adequately the experimental procedure. In no case does such identification imply recommendation by the National Institute of Standards and Technology nor does it imply that the material or equipment identified is necessarily the best available for this purpose.
(54) Smith, D. R.; Meier, D. J. *Polymer* **1992**, *33* (18), 3777–3782.
(55) Stafford, C. M.; Roskov, K. E.; Epps, T. H., III; Fasolka, M. J. *Rev. Sci. Instrum.* **2006**, *77* (2), 023908.
(56) *Polymer Handbook*, 4th ed.; John Wiley & Sons, Inc.: Hoboken, 1999; Vol. 2.
(57) Harrison, C.; Cabral, J. T.; Stafford, C. M.; Karim, A.; Amis, E. J. *J. Micromech. Microeng.* **2004**, *14*, 153–158.
(58) Cabral, J. T.; Hudson, S. D.; Harrison, C.; Douglas, J. F. *Langmuir* **2004**, *20*, 10020–10029.
(59) Truong, T. T.; Lin, R.; Jeon, S.; Lee, H. H.; Maria, J.; Gaur, A.; Hua, F.; Meinel, I.; Rogers, J. A. *Langmuir* **2007**, *23* (5), 2898–2905.
(60) *NIST Chemistry WebBook, NIST Standard Reference Database Number 69*; Linstrom, P. J., Mallard, W. G., Eds., National Institute of Standards and Technology: Gaithersburg, MD, 20899.
(61) Knoll, A.; Magerle, R.; Krausch, G. *Macromolecules* **2001**, *34* (12), 4159–4165.
(62) Kim, H.-C.; Russell, T. P. *J. Polym. Sci., Part B: Polym. Phys.* **2001**, *39*, 663–668.
(63) Matsen, M. W.; Schick, M. *Phys. Rev. Lett.* **1994**, *72* (16), 2660–2663.
(64) Cochran, E. W.; Garcia-Cervera, C. J.; Fredrickson, G. H. *Macromolecules* **2006**, *39* (7), 2449–2451.
(65) Matsen, M. W.; Thompson, R. B. *J. Chem. Phys.* **1999**, *111*, 7139–7146.
(66) Croll, S. G. *J. Appl. Polym. Sci.* **1979**, *23*, 847–858.
(67) Roskov, K. E.; Epps, T. H., III; Berry, B. C.; Hudson, S. D.; Tureau, M. S.; Fasolka, M. J. *J. Comb. Chem.* **2008**, *10* (6), 966–973.